Title: Tuning the composition of porous resin-templated TiO_2 macrobeads for optimized photocatalytic performance

Authors: Q.A. Naqvi, M. Ratova, R. Klaysri, P.J. Kelly, M. Edge, S. Potgieter-Vermaak, L. Tosheva

PII: S0920-5861(18)30755-7
DOI: https://doi.org/10.1016/j.cattod.2018.06.031
Reference: CATTOD 11520

To appear in: *Catalysis Today*

Received date: 31-1-2018
Revised date: 29-5-2018
Accepted date: 15-6-2018

Please cite this article as: Naqvi QA, Ratova M, Klaysri R, Kelly PJ, Edge M, Potgieter-Vermaak S, Tosheva L, Tuning the composition of porous resin-templated TiO_2 macrobeads for optimized photocatalytic performance, *Catalysis Today* (2018), https://doi.org/10.1016/j.cattod.2018.06.031

Tuning the composition of porous resin-templated TiO_2 macrobeads for optimized photocatalytic performance

Q. A. Naqvi[1], M. Ratova[1], R. Klaysri[1,2], P. J. Kelly[1], M. Edge[1], S. Potgieter-Vermaak[1,3], and L. Tosheva[1,*]

[1] Faculty of Science and Engineering, Manchester Metropolitan University, Chester Street, Manchester, M1 5GD, United Kingdom

[2] Center of Excellence on Catalysis and Catalytic Reaction Engineering, Department of Chemical Engineering, Faculty of Engineering, Chulalongkorn University, Bangkok 10330, Thailand

[3] Molecular Science Institute, School of Chemistry, University of the Witwatersrand, P.O. Box X3, Wits, 2050, South Africa

*Corresponding author. *E-mail address:* l.tosheva@mmu.ac.uk (L. Tosheva)

Graphical Abstract

Highlights

- Porous TiO_2 beads are prepared by resin templating.
- The anatase/rutile bead composition can be varied through synthesis parameters.
- TiO_2 beads show higher charge carrier generation and retarded charge recombination.

ABSTRACT

TiO_2 in the form of macroscopic beads was prepared by resin templating. Anion-exchange macroporous resin beads were treated with a synthesis gel containing titanium isopropoxide, iso-propanol and diluted (0-5 wt.%) tetrapropylammonium hydroxide (TPAOH) aqueous solutions. The Ti-resin composite obtained was calcined at 600 °C to remove the resin. The presence of TPAOH in the precursor solution was essential for producing intact TiO_2 beads. The use of 1-1.5 wt.% TPAOH resulted in anatase beads, whereas further increase in the TPAOH content promoted the anatase to rutile phase transformations. Decreasing the heating rate used during calcination also resulted in changes in the TiO_2 composition from pure anatase (16 °C min^{-1} heating rate) to anatase with rutile impurities (0.5 °C min^{-1} heating rate). The photocatalytic activity of the TiO_2 beads was evaluated for the degradation of acetone under ultraviolet irradiation. A high activity was displayed by the TiO_2 samples composed of anatase with rutile impurities, whereas the activity was lower for pure anatase samples or samples containing mainly rutile. The TiO_2 beads showed higher rates of charge carrier generation and slower charge trapping/recombination rates compared to a reference Cristal ACTiV™ PC500. In addition, the TiO_2 beads could be used in at least five consecutive catalytic cycles without any in-between cycle treatment, without significant changes in their activity.

Keywords: Resin templating; TiO_2; Porous beads; Photocatalysis; Acetone degradation

1. Introduction

Owing to their high stability, non-toxicity and high catalytic activity under ultraviolet (UV) radiation, TiO_2 nanopowders have been widely used as photocatalytic materials for the degradation of organic pollutants and hydrogen production [1,2]. In the quest to enhance the photocatalytic performance of these materials and to increase their catalytic lifetime, recent research efforts have been focused on optimizing the composition of TiO_2 materials, their morphology and their macroscopic shape. Thus, composites of TiO_2 nanoparticles with other materials such as zeolite-templated carbon [3], zeolite and mesoporous silica [4,5], graphene [6] and carbon nanotubes [7] have been prepared with superior photocatalytic activity, due to the greater adsorptive properties of the composites and delayed electron/hole recombination. Introduction of hierarchical porosity can further improve the diffusion of reactants, facilitate accessibility of inner active sites and enhance light harvesting [8]. Porous titania networks containing interconnected meso- and macropores have been prepared by templating approaches using organic, e.g., hexadecylamine, agarose and polymer beads, or mixed silica-surfactant templates [9-12].

A major drawback in the application of nanomaterials in liquid-phase reactions is the difficulty in recovering the particulate nanocatalysts, which usually requires high-speed centrifugation and results in material loss during transfers. TiO_2 in the form of monoliths have been prepared by templating methods to overcome this issue [13-16]. Macroscopic porous structures in the form of spherical particles are particularly advantageous for applications in fixed-bed reactors and chromatography columns due to

improved mass transfer, reduced pressure-drop and attrition resistance. The resin-templating method is one of the most versatile methods used for the preparation of porous inorganic beads. Macroreticular ion-exchange resins are comprised of tiny gel particles with a size of ca. 100 nm, which form a rigid pore network within each resin bead [17]. The ion-exchange capacity of the resin can be used to introduce the desired inorganic precursor phase within the resin, most often through anion-exchange. Upon calcination, the resin is removed, leaving behind inorganic beads with secondary porosity due to resin removal.

We have used the resin-templating method to prepare different types of zeolites, including TS-1 [18-20]. The latter materials showed potential to slow down the recombination of trapped charges upon UV radiation, which was attributed to the hierarchical porosity of the beads. TS-1 and amorphous titanosilicate beads have been prepared by others using anion-exchange resins as templates [21-23]. Amorphous titanosilicate beads containing a certain amount of anatase at high TiO_2 loading showed potential for use in the photocatalytic degradation of phenol, although no correlation has been found between the Ti content and the photocatalytic activity [24]. Composite TiO_2/carbon beads have been prepared by an impregnation-carbonization method and tested for the photocatalytic degradation of methyl orange under visible light radiation [25]. Anatase beads have been prepared using cation-exchange resins via intermediate hydroxide precipitation of pre-loaded metal salts with ammonia [26]. The TiO_2 beads contained large macropores, which were not observed in materials prepared with anion-exchange resins, however, the materials have not been tested as potential catalytic materials.

Some of the above works suggest that the resin templating method can be used to prepare porous beads with photocatalytic activity. The resin combustion yields the unique porous structure of these materials, yet, the influence of calcination conditions such as heating rates has not been studied before. Further, the application of such beads in photocatalytic reactions in the gas phase has not been explored so far. The presence of volatile organic compounds (VOCs) in indoor air has an increasing impact on human health. Photocatalytic deep oxidation of VOCs to CO_2 and H_2O is amongst the most promising technologies for purification of indoor air due to its features such as room temperature operation, non-specificity towards reactants and benign end products [27-29]. The use of photocatalysts in the form of macroscopic beads in such applications would be particularly beneficial due to their increased attrition resistance and minimized risks of air contamination. The aims of this work were to prepare TiO_2 beads by resin templating and to tune their morphology and phase composition for optimized performance in the photocatalytic decomposition of acetone as a model VOC under UV irradiation. Parameters such as the chemical composition of the precursor TiO_2 gel and the heating rate used to reach the resin combustion temperature were studied.

2. Experimental section

2.1. Preparation of resin-templated TiO_2 beads

A strongly basic anion-exchange resin (Amberlite IRA-900, Sigma-Aldrich) was used as a sacrificial macrotemplate in all experiments. The required amount of resin was weighed and converted from chloride to hydroxide form by rinsing three times with 0.1 M NaOH solution (NaOH pellets, ≥98%, Sigma-Aldrich). This was followed by rinsing three times with distilled water and removing excess water with a plastic pipette. The TiO_2 precursor solution was then added to the resin at a weight ratio of 10 to 1, the

mixture was transferred to a polypropylene reactor and treated at 60 °C for 24 h. For the TiO_2 precursor solution, titanium (IV) isopropoxide (Ti-iso, 95%, Alfa Aesar) was added to propan-2-ol (PrOH, HPLC grade, Fisher Scientific; the alcohol was dried over 4A molecular sieve prior to use) and stirred for 15 min. Distilled water or diluted aqueous tetra-n-propyl ammonium hydroxide solutions (TPAOH, 1 M aqueous solution, Alfa Aesar), 1, 1.5, 2 or 5 wt.% TPAOH, were then added dropwise (1 ml min^{-1}) to the clear mixture, which resulted in the formation of a white gel, and stirring continued for 1 h. The molar compositions of the TiO_2 precursor mixtures were 1.00Ti-iso : 9.51PrOH: *x*TPAOH : *y*H_2O, where *x*=0, 0.10, 0.15, 0.20 or 0.49 and *y*=111.11, 110.00, 109.44, 108.89 or 105.56, corresponding to the different TPAOH concentrations used (0, 1, 1.5, 2 and 5 wt.% TPAOH). After the treatment, the resin/Ti composite was separated from the mother liquor by decanting, rinsed several times with distilled water and dried at 60 °C overnight. The resin was removed by calcination at 600 °C for 10 h after heating to this temperature at heating rates of 0.5, 5, 10 or 16 °C min^{-1}. The crucibles were covered loosely with lids during calcination to avoid losing material/sample contamination during the resin combustion.

2.2. Characterization

The morphology of the TiO_2 beads was studied by scanning electron microscopy (SEM, JEOL 5600LV scanning electron microscope). X-ray diffraction (XRD) patterns were measured with an X'Pert PANalytical X-ray diffractometer, employing Cu Kα radiation (40 kV and 30 mA) and a PIXcell detector. Samples were ground into a powder in an agate mortar prior to XRD analysis. Crystallite sizes were determined in HighScore by Rietveld refinement with a CeO_2 sample collected using the same collection parameters used as the instrument standard. The porous structure of the TiO_2 samples was studied

by nitrogen adsorption-desorption measurements at -196 °C with a Micromeritics ASAP 2020 surface area analyzer. Samples were degassed at 200 °C overnight prior to analysis. The surface areas were calculated using the BET equation and pore size distributions were obtained by the BJH method from the desorption branch of the isotherms. The total pore volume of the samples was calculated by converting the volume adsorbed at a relative pressure of 0.995 to the volume of liquid adsorbate. UV-vis spectra of ground samples were recorded with a Cary 100 UV-vis spectrophotometer equipped with an internal G9830A Diffuse Reflectance Accessory (Agilent Technologies) using a white USRS-99-010 standard reference material for background correction. The band gap values of the samples were calculated from Tauc plots using the Kubelka-Munk function F(R).

2.3. Acetone degradation test

The photocatalytic activity of the TiO_2 beads was evaluated using acetone degradation test, developed in-house [30]. In this test, a fixed amount of sample (0.3 g) was spread over a 55 mm petri dish and placed into a purpose-built reaction cell. Liquid acetone (3 ml) was injected into the cell and the mixture was kept in the dark for 30 min to reach equilibrium. The beads were then exposed to UV radiation (2 x 15 W 352 nm Sankyo Denki BLB lamps) for 1 h. The CO_2 concentration during irradiation was measured with a Vaisala CARBOCAP® carbon dioxide meter used with a Vaisala GM70 2000 ppm probe. The evolution of CO_2 over time ($[CO_2]$/time gradient) was used as a measure of the photocatalytic activity of the samples [31]. The sample prepared with 1.5 wt.% TPAOH and a heating rate of 5 °C min^{-1} was selected for further photocatalytic studies. First, an acetone degradation test was performed as above but using 1 g of TiO_2 beads and the test was repeated with 1 g of CristalACTiV™ PC500 (Cristal) to

qualitatively compare the performance of the two samples. PC500 has been reported to be more active than Evonik P25 for gas-phase photocatalytic oxidations, which was the reason for selecting it as a reference in this work [32]. Second, the reusability of the TiO_2 beads was tested by running five consecutive catalytic cycles. The experiment was performed by injection of 3 ml of acetone using 1 g of TiO_2 beads, conditioning for 30 min in the dark and then unblocking the light path and irradiating for 1 h. After the cycle, the sample was taken out of the test chamber, the chamber was flushed with compressed air to remove the CO_2 (as judged from the readout of the CO_2 probe), the sample was returned to the test chamber and the test was repeated. The whole experiment was completed on the same day.

Microwave broadband dielectric loss (BDS) measurements were carried out using a Marconi IFR 6823 programmable scalar analyser connected to a rectangular waveguide and cylindrical cavity [33, 34]. Reference anatase nanopowder (Cristal ACTiV™ PC500, Cristal) and the TiO_2 sample prepared with 1.5 wt.% TPAOH and 5 °C min^{-1} heating rate (1.0 g) were placed in the cavity and irradiated with a visible light source (60 W, tungsten). This irradiation results in a shift of the resonant frequency position and attenuation of the microwave power due to the production of heat (phonons) by free carriers; these changes are proportional to the number of free-carriers produced. The time dependence of the attenuation of the microwave power (± 0.05 dBm) provides a profile of the production of free charge carriers during irradiation. Upon switching off the light, the rate of charge carrier recombinations can be studied. The microwave power stored by the microwave cavity (dBm m^{-2}) was monitored at room temperature in real-time during 1800 s of irradiation and then for a further 1800 s with the light-source switched-off for each of the two samples.

3. Results and discussion

2.4. Synthesis and optimization of TiO_2 beads

The TiO_2 samples prepared in this work were optimized in terms of their macroscopic shape and TiO_2 crystalline phases. Two factors were found to influence these properties, namely the presence of TPAOH in the synthesis gel and the heating rate used during calcination. A description of the samples prepared by varying these two parameters is presented in Table 1.

First, TiO_2 samples were prepared from synthesis gels containing 0-5 wt.% TPAOH using a heating rate of 5 °C min^{-1}. The sample prepared in the absence of TPAOH consisted of flakes and aggregates (Fig. 1a). Some disintegrated particles were present in the sample prepared with 1 wt.% TPAOH and the particles appeared to be hollow (Fig. 1b). Such hollow particles have been observed before for the synthesis of ZSM-5 by resin templating [35]. The effect was attributed to preferential crystal growth at the surface of the resin at the expense of nutrients from the resin's interior under certain experimental conditions, leaving behind hollow particles upon resin removal. The samples prepared with 1.5, 2 and 5 wt.% TPAOH were composed of intact beads (Fig. 1c-e). The beads prepared with 5 wt.% TPAOH were similar in size to the original resin beads (Fig. 1e and f, correspondingly), whereas the 1.5 and 2 wt.% beads were smaller. Similar results have been reported previously for the influence of TPAOH on the macroscopic shape of samples prepared by resin templating [36]. The different morphologies of the samples prepared with different amounts of TPAOH may be due to two factors. First, increasing the TPAOH concentration leads to an increase of the pH of the precursor solution, resulting in a supressed polycondensation and a more negative surface of the TiO_2 species [37], both of which facilitate the ion-exchange of TiO_2

within the resin. Second, TPA cations are a well-known structure-directing template in the synthesis of MFI-type zeolites through their specific interactions with condensed silica to form pre-nucleation inorganic-organic species [38]. Similar interactions may occur between TPAOH and Ti species during the hydrolysis and condensation of titanium isopropoxide.

XRD patterns of the samples prepared using different TPAOH content are shown in Fig. 2. The XRD analysis of Ti-resin composite samples showed the presence of poorly resolved diffraction peaks, indicating the formation of amorphous TiO_2 clusters. The calcined samples contained anatase (1 and 1.5 wt.% TPAOH), anatase-rutile (2 wt.% TPAOH) or rutile-anatase (the samples prepared in the absence of TPAOH and in the presence of 5 wt.% TPAOH, correspondingly). Pure anatase samples were prepared with 1 wt.% and 1.5 wt.% TPAOH. According to Table 1, these two samples showed the highest BET surface areas, about 40 $m^2 g^{-1}$. The anatase crystallites in these two samples were ca. 30 nm, which increased in size to > 40 nm in the 2 wt.% and 5 wt.% TPAOH samples (Table S1). Thus, a possible explanation for the differences observed for samples prepared with different TPAOH content might be that a higher porosity results in retardation of the anatase to rutile transformation due to a reduction in the anatase-anatase interface [10, 39]. The rutile content increases in the order 2 wt.% TPAOH < No TPAOH < 5 wt.% TPAOH, and the surface areas decrease in the same order, which further confirms this hypothesis.

Further details about the porous structure of the samples prepared with different amount of TPAOH were obtained from nitrogen adsorption data (Fig. S1 and Table 1). The mesopores of the sample prepared in the absence of TPAOH were disordered in accordance with the disintegration of the spherical structure of this sample observed by

SEM (Fig. 1 a). The BJH mesopore peak for all samples was centred at about 25 nm and there were variations in its height and width between the samples. Except for the No TPAOH and 1 wt.% TPAOH samples, which, according to SEM were not solid, all other samples showed comparable total pore volumes. Negligible micropore volumes (< 0.001 $cm^3 g^{-1}$) were detected by the t-plot method in samples 2, 4 and 5, indicating that the total pore volume was solely due to the removal of the resin. The variations in the surface area and total pore volumes of the TiO_2 beads can be related to variations in the anatase/rutile ratios and variations in corresponding crystallite sizes. The sample prepared using 1.5 wt.% TPAOH was selected for optimization of the heating rate used during calcination.

SEM images of samples prepared with 1.5 wt.% TPAOH and different heating rates are shown in Fig. S2. For these experiments, a batch of Ti-resin composite was prepared and split into four samples, which were calcined at different heating rates. All samples, except the 0.5 °C min^{-1}, contained intact spherical beads. The smoothness of the beads' surface increased with an increase in the heating rate. Similar trends were obtained for beads prepared with 2 wt.% and 5wt.% TPAOH (Fig. S3). The XRD analysis indicated that the 5, 10 and 16 °C min^{-1} samples consisted of anatase, whereas the 0.5 °C min^{-1} contained rutile impurities (Fig. S4). Raman spectroscopy was further used to characterize the samples prepared with different heating rates as a more sensitive method for detection of crystalline TiO_2 phases [40]. Raman spectra of at least 50 particles of each sample were collected and four representative areas were identified as shown in Fig. 3, characteristic of pure anatase (Area 1) and anatase containing different amounts of rutile (Areas 2-4). The sample calcined using a heating rate of 16 °C min^{-1} contained pure anatase without any impurities of rutile. The amount of rutile

increased with a decrease in the heating rate as observed from the increase in the intensity of the most intense rutile Raman band at the 608 ± 4 cm^{-1} position (symmetric O-Ti-O stretching vibrational mode). However, it was not possible to determine quantitatively the exact fraction of rutile in the samples due to the their inhomogeneity. The differences observed in the morphology and structure of samples prepared with different heating rates may be related to: (i) a less efficient heat transfer at higher heating rates and (ii) differences in diffusion of heat / decomposition of gases during the removal of the substantial amount of organic matter [41].

2.5. Photocatalytic degradation of acetone

The photocatalytic activity of the TiO_2 samples prepared was studied using the acetone degradation test (Fig. 4 and Table 1) [31]. Various factors can influence the photocatalytic activity of TiO_2 materials, such as their electronic and morphological properties [42]. A synergistic effect has been reported between anatase and rutile for anatase samples containing up to 40% rutile [43, 44]. On the other hand, different photocatalytic activities have been determined for TiO_2-catalysed reactions in the gas phase and liquid-state reactions [32].

The band gaps reported in Table 1 are in agreement with the XRD and Raman results and literature values for anatase and anatase/rutile mixtures [43]. The results of the photocatalytic tests indicate that: (i) the samples that contained mainly rutile (samples 1 and 5) displayed lower activity; (ii) sample 2 showed high activity, but this sample had different morphology compared to the other TiO_2 beads; (iii) the increase in the [CO_2]/time gradient for the rest of the TiO_2 beads was proportional to the total pore volume of the samples, although the composition was important as well and samples 4 (anatase + rutile) and 8 (pure anatase) were less active compared to samples 3, 6 and 7.

The sample prepared with 1.5 wt.% TPAOH and 5 °C min^{-1} (sample 3) was selected for a qualitative comparison with the reference PC500 sample. The results of the photocatalytic tests indicated that the TiO_2 beads were about twice more active compared to the reference PC500 powder (not shown). The two samples were very different in nature in terms of composition and surface area. PC500 has a crystallite size of 5-10 nm, a surface area of 345 m^2 g^{-1} and contains anatase (85 wt.%) and an amorphous material. Nevertheless, the comparison suggests that the beads developed in this work are highly active in gas-phase photocatalytic oxidation reactions.

It is known that the separation efficiency of free charge carriers is an extremely important factor for enhancement of the photocatalytic activity. Therefore, the higher photocatalytic activity of the TiO_2 beads, in terms of acetone degradation, can be partly attributed to the longer lifetime of photo-generated charge carriers, rather than simply to a reduction in the band gap (the band gap of PC500 is 3.20 eV). The attenuation of cavity microwave power for PC500 and the TiO_2 beads is given in Fig. 5. During the light-on cycle, higher rates of charge carrier generation are evident, as reflected by the attenuation of the cavity power. The two samples clearly exhibit different dynamics of charge carrier generation and relaxation. For PC500, there is an initial rapid attenuation of microwave power consistent with an injection of free-carriers. However, within a few seconds the power levels-off suggesting an equilibrium between free-carrier generation and carrier recombination/trapping has been established. The very high surface area of the sample (345 m^2 g^{-1}) is consistent with this observation. Conversely, the attenuation of power for the TiO_2 beads continues to steadily increase during the timeframe of irradiation (1800 s). This suggests that there is continual production of free-carriers that does not undergo recombination/trapping during irradiation, i.e. there is efficient

separation of free charge carriers. It is apparent that trapping/recombination occurs on a much faster timescale for PC500 than for the beads. Once the light is turned-off, there is a rapid reduction in attenuation of power for PC500 consistent with recombination/trapping of free carriers. The fact that there is a residual attenuation of power suggests that, at room temperature, some free-carriers remain in the sample during the timeframe of the experiment. For the TiO_2 beads, recombination/trapping of free-carriers occurs on a slower timescale and it is clear that a significant number of charge carriers persist in this material after the light has been switched-off. These results can be directly related to the composition of the TiO_2 beads and their porous structure.

Finally, the reusability of the beads was tested by running five consecutive catalytic cycles (Fig. 6). The acetone degradation rate is slightly lower for the first run, which could be due to contamination caused by adsorbed species during storage. The rates after the first run are similar, which indicate that the sample can be reused in at least five cycles without any regeneration required between cycles.

Conclusions

Porous TiO_2 beads were prepared by resin templating using a macroporous anion-exchange resin. The presence of TPAOH was essential for the synthesis of intact TiO_2 beads. The amount of rutile in the beads increased with an increase in the TPAOH concentration, which was related to the lower porosity of corresponding samples facilitating anatase to rutile transformations. Decreasing the heating rate during calcination resulted in changes in the surface composition of the beads from pure anatase to anatase containing rutile impurities, as indicated by Raman analysis. Variations in the structural composition resulted in variations in the textural

characteristics of the samples, which affected their photocatlytic activity as determined using an acetone degradation test. Pure anatase beads and beads containing mainly rutile were found to be less active, compared to anatase beads with rutile impurities. A qualitative comparison of a representative TiO_2 sample with a reference TiO_2 nanopowder (CristalACTiV™ PC500) showed that the TiO_2 beads displayed higher activity, which was attributed to their more efficient charge carrier generation and retarded charge recombination. The macroscopic shape of the TiO_2 beads prepared in this work makes them superior compared to commercial TiO_2 powders in photocatalytic applications in the gas-phase due to minimized loss of material during transfers, minimized risks of dust inhalation and easy handling.

Acknowledgements

The authors are grateful to Dr Gary Miller (MMU) for performing the Rietveld refinement.

References

[1] X. Chen, S.S. Mao, Chem. Rev. 107 (2007) 2891-2959.

[2] J. Schneider, M. Matsuoka, M. Takeuchi, J. Zhang, Y. Horiuchi, M. Anpo, D.W. Bahnemann, Chem. Rev. 114 (2014) 9919-9986.

[3] W. Donphai, T. Kamegawa, M. Chareonpanich, K. Nueangnoraj, H. Nishihara, T. Kyotani, H. Yamashita, Phys. Chem. Chem. Phys. 16 (2014) 25004-25007.

[4] I. Jansson, S. Suárez, F. Javier Garcia-Garcia, B. Sánchez, Appl. Catal. B 178 (2015) 100-107.

[5] C. Jiang, K.Y. Lee, C.M.A. Parlett, M.K. Bayazzit, C.C. Lau, Q. Ruan, S.J.A. Moniz, A.F. Lee, J. Tang, Appl. Catal. A 521 (2016) 133-139.

[6] P. Shengyan, Z. Rongxin, M. Hui, D. Daili, P. Xiangjun, Q.F.C. Wei, Appl. Catal. B 218 (2017) 208-219.

[7] K. Woan, G. Pyrgiotakis, W. Sigmund, Adv. Mater. 21 (2009) 2233-2239.

[8] W. Jiang, Y. Zhu, G. Zhu, Z. Zhang, X. Chen, W. Yao, J. Mater. Chem. A 5 (2017) 5661-5679.

[9] L. Cao, D. Chen, W.-Q. Wu, J.Z.Y. Tan, R.A. Caruso, J. Mater. Chem. A 5 (2017) 3645-3654.

[10] L. Cao, D. Chen, W. Li, R.A. Caruso, ACS Appl. Mater. Interfaces 6 (2014) 13129-13137.

[11] U. Meyer, A. Larsson, H.-P. Hentze, R.A. Caruso. Adv. Mater. 14 (2002) 1768-1772.

[12] W. Dong, Y. Yao, L. Li, Y. Sun, W. Hua, G. Zhuang, D. Zhao, S. Yan, W. Song, Appl. Catal. B 217 (2017) 293-302.

[13] K. Nakata, T. Kagawa, M. Sakai, S. Liu, T. Ochiai, H. Sakai, T. Murakami, M. Abe, A. Fujishima, ACS Appl. Mater. Interfaces 5 (2013) 500-504.

[14] T. Long, L. Xu, T. Zhang, Y. Wang, Mater. Manuf. Process. 29 (2014) 743-747.

[15] N.M. Nursam, X. Wang, J.Z.Y. Tan, R.A. Caruso, ACS Appl. Mater. Interfaces 8 (2016) 17194-17204.

[16] J. Gjipalaj, I. Alessandri, J. Env. Chem. Eng. 5 (2017) 1763-1770.

[17] D.C. Sherrington, Chem. Commun. (1998) 2275-2286.

[18] L. Tosheva, V. Valtchev, J. Sterte, Microporous Mesoporous Mater. 35–36 (2000) 621–629.

[19] V. Naydenov, L. Tosheva, O.N. Antzutkin, J. Sterte, Microporous Mesoporous Mater. 78 (2005) 181-188.

[20] S.P.D. Ormond, M. Ratova, P. Kelly, M. Edge, B. Mihailova, L. Tosheva, J. Porous Mater. 23(2006) 1421-1429.

[21] W. Cheng,Y. Jiang, X. Xu, Y. Wang, K. Lin, P.P. Pescarmona, J. Catal. 333 (2016) 139-148.

[22] K. Lin, O.I. Lebedev, G. Van Tendeloo, P.A. Jacobs, P.P. Pescarmona, Chem. Eur. J. 16 (2010) 13509-13518.

[23] S. Zhang, Y. Jianga, S. Li, X. Xu, K. Lina, Appl. Catal. A 490 (2015) 57-64.

[24] D. Cani, P.P. Pescarmona, J. Catal. 311 (2014) 404-411.

[25] X. Li, Y. Jiang, W. Cheng, Y. Li, X. Xu, K. Lin, Nano-Micro Lett. 7 (2015) 243-254.

[26] M.-L. Wang, C.-H. Wang, W. Wang, J. Mater. Chem. 17 (2007) 2133-2138.

[27] A.H. Mamaghani, F. Haghighat, C.-S. Lee, Appl. Catal. B 203 (2007) 247-269.

[28] Y. Boyjoo, H. Sun, J. Liu, V.K. Pareek, S. Wang, Chem. Eng. J. 310 (2017) 537-559.

[29] Y. Huang, S.S.H. Ho, Y. Lu, R. Niu, L. Xu, J. Cao, S. Lee, Molecules 21 (2016) 56.

[30] M. Ratova, P.J. Kelly, G.T. West, L. Tosheva, M. Edge, Appl. Surf. Sci. 392 (2017) 590-597.

[31] A. Torras-Rosell, S.R. Johannsen, K. Dirscherl, S. Daviðsdóttir,·C.S. Jeppesen, S. Louring, I.H. Andersen, Environ. Sci. Pollut. Res. 24 (2017) 12683–12690.

[32] S.W. Verbruggen, K. Masschaele, E. Moortgat, T.E. Korany, B. Hauchecorne, J.A. Martens, S. Lenaerts, Catal. Sci. Technol. 2 (2012) 2311-2318.

[33] M. Edge, R. Janes, J. Robinson, N. Allen, F. Thompson, J. Warman, J. Photochem. Photobiol. A 113 (1998) 171-180.

[34] J. Verran, G. Sandoval, N.S. Allen, M. Edge, J. Stratton, Dyes Pigm. 73 (2007) 298-304.

[35] L. Tosheva, J. Sterte, Surf. Sci. Catal. 142 (2002) 183-189.

[36] L. Tosheva, V. Valtchev, J. Sterte, J. Mater. Chem. 10 (2000) 2330-2336.

[37] B. Tryba, M. Tygielska, C. Colbeau-Justin, E. Kusiak-Nejman, J. Kapica-Kozar, R. Wróbel, G. Z. Zołnierkiewicz, N. Guskos, Mater. Res. Bull. 84 (2016) 152-161.

[38] S.L. Burkett, M.E. Davis, Chem. Mater. 7 (1995) 920-928.

[39] J. Zhang, M. Li, Z. Feng, J. Chen, C. Li, J. Phys. Chem. 110 (2006) 927-935.

[40] X. Gao, S.R. Bare, J.L.G. Fierro, M.A. Banares, I.E. Wachs, J. Phys. Chem B 102 (1998) 5653-5666.

[41] J.M. Encinar, J.F. González, Fuel Process. Technol. 89 (2008) 678-686.

[42] M. Keulemans, S.W. Verbruggen, B. Hauchecorne, J.A. Martens, J. Catal. 344 (2016) 221-228.

[43] R.I. Bickley, T. Gonzales-Carreno, J.S. Lees, L. Palmisano, R.J.D. Tilley, J. Solid State Chem. 92 (1991) 178-190.

[44] R. Su, R. Bechstein, L. Sø, R.T. Vang, M. Sillassen, B. Esbjörnsson, A. Palmqvist, F. Besenbacher, J. Phys. Chem. C 115 (2011) 24287-24292.

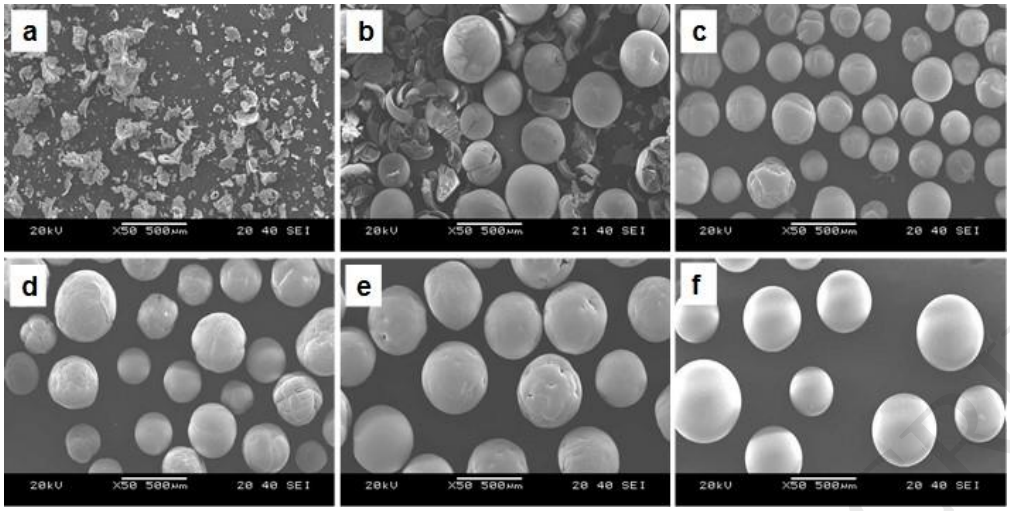

Fig. 1. SEM images of samples prepared using: (a) 0 wt.%, (b) 1 wt.%, (c) 1.5 wt.%, (d) 2 wt.% and (e) 5 wt.% TPAOH, and (f) the original resin beads.

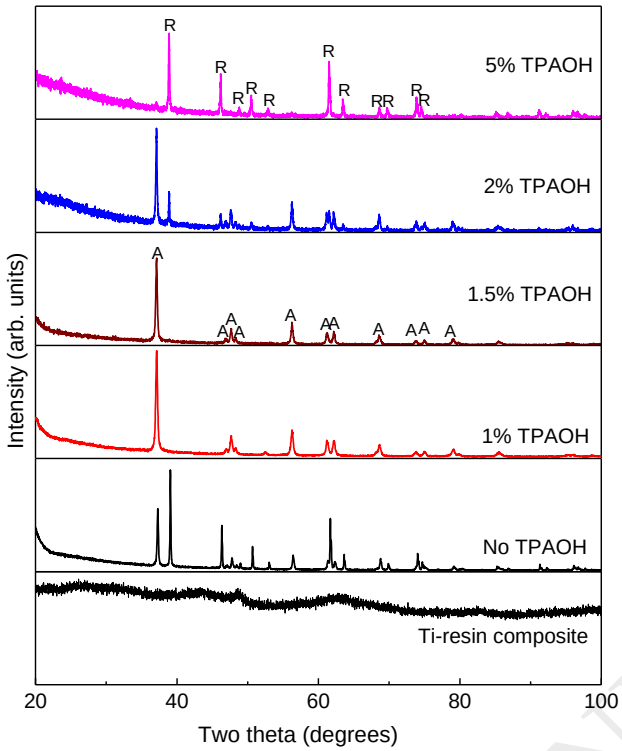

Fig. 2. XRD patterns of calcined TiO_2 samples prepared from gels containing different amount of TPAOH. The bottom XRD pattern shows a typical XRD pattern of a Ti-resin composite.

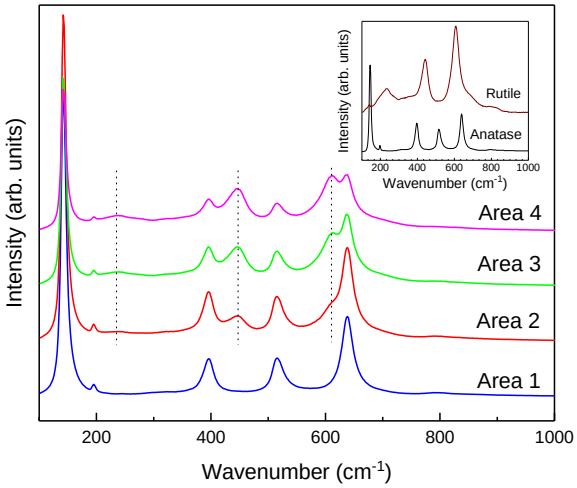

Fig. 3. Representative Raman spectra collected from the TiO_2 beads prepared using different heating rates. The insert shows the reference Raman spectra of rutile and anatase.

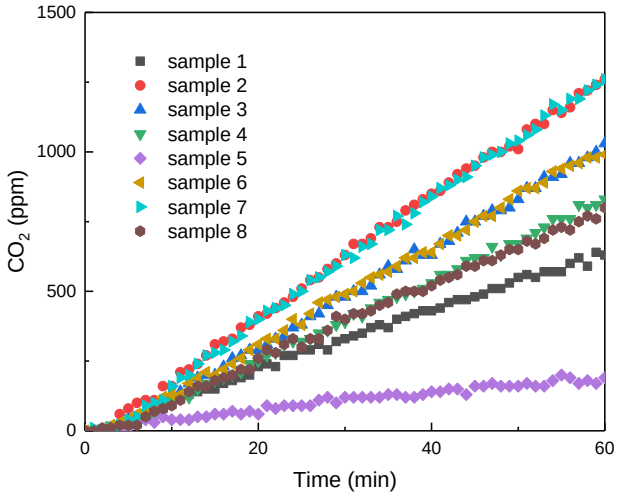

Fig. 4. Acetone degradation tests for the TiO_2 samples described in Table 1.

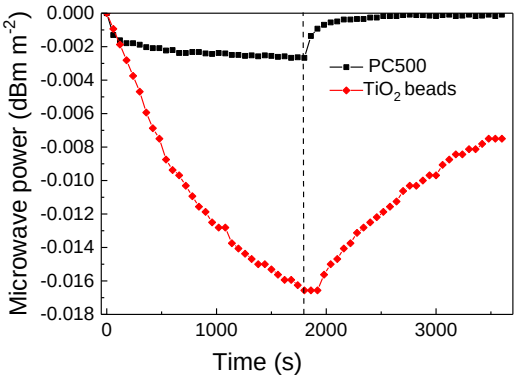

Fig. 5. Microwave power in microwave cavity with irradiation for 1800 s followed by switching off the light source for PC500 and TiO_2 beads (1.5 wt.% TPAOH and 5 °C min^{-1} heating rate).

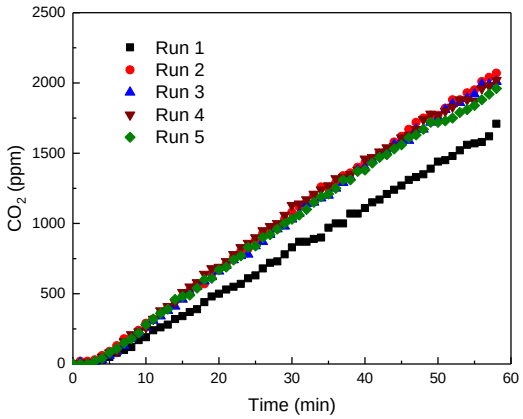

Fig. 6. Five consecutive runs of the acetone degradation test over the sample prepared with 1.5 wt.% TPAOH and 5 °C min^{-1} heating rate.

Table 1 Sample description, BET surface areas (S_{BET}), total pore volumes (V_p), band gaps and evolution of CO_2 as a function of time gradient of the TiO_2 samples prepared.

Sample	Heating rate (°C min^{-1})	TPAOH (wt.%)	S_{BET} (m^2 g^{-1})	V_p (cm^3 g^{-1})	Band gap (eV)	$[CO_2]$/time gradient (ppm min^{-1})
1	5	-	7	0.l3	2.92	11.0
2	5	1	37	0.57	3.10	21.8
3	5	1.5	40	0.32	3.06	17.7
4	5	2	21	0.31	2.94	14.4
5	5	5	5	0.27	2.92	3.2
6	0.5	1.5	35	0.34	2.94	17.5
7	10	1.5	38	0.36	3.06	22.0
8	16	1.5	24	0.30	3.04	13.7